Conf-780314 8

PREPRINT UCRL-79539, Rev. 1

A TWO-DIMENSIONAL COMPUTER SIMULATION OF HYPERVELOCITY IMPACT CRATERING: SOME PRELIMINARY RESULTS FOR MEteor CRATER, ARIZONA

J. B. Bryan, D. E. Burton, M. F. Cunningham, and L. A. Lettis, Jr.

June 1978

MASTER

This paper was prepared for submission to the Ninth Lunar and Planetary Science Conference, Houston, TX, March 13-17, 1978

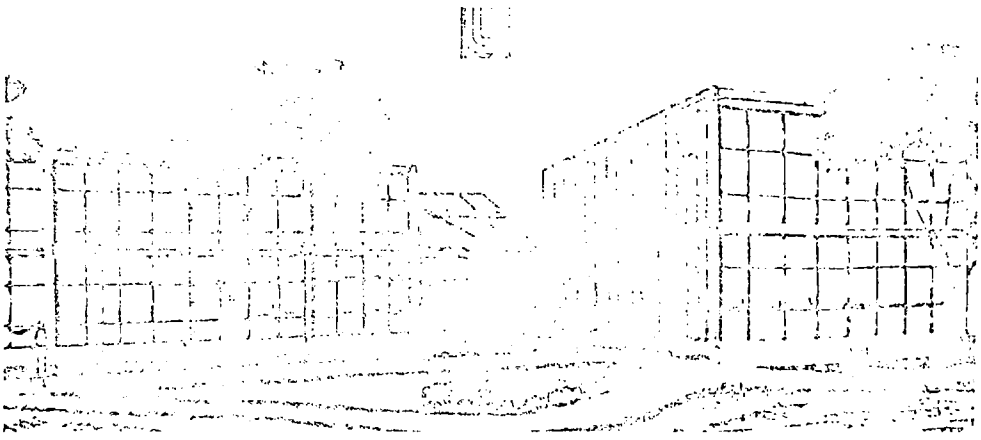

A TWO-DIMENSIONAL COMPUTER SIMULATION OF HYPERVELOCITY IMPACT CRATERING: SOME PRELIMINARY RESULTS FOR METEOR CRATER, ARIZONA*

J. L. Bryan, D. L. Burton, M. E. Cunningham, and L. A. Lettis, Jr.

Earth Sciences Division
Lawrence Livermore Laboratory, University of California
Livermore, California 94550

ABSTRACT

A computational approach used for subsurface explosion cratering has been extended to hypervelocity impact cratering. Meteor (Barringer) Crater, Arizona, was selected for our first computer simulation because it is one of the most thoroughly studied craters. It is also an excellent example of a simple, bowl-shaped crater and is one of the youngest terrestrial impact craters. Initial conditions for this calculation included a meteorite impact velocity of 15 km/s, meteorite mass of 1.67×10^{8} kg, with a corresponding kinetic energy of 1.88×10^{16} J (4.5 megatons). A two-dimensional Eulerian finite difference code called SOIL was used for this simulation of a cylindrical iron projectile impacting at normal incidence into a limestone target. For this initial calculation, a Tillotson equation-of-state description for iron and limestone was used with no shear strength. Results obtained for this preliminary calculation of the formation of Meteor Crater are in good agreement with field measurements. A color movie based on this calculation was produced using computer-generated graphics.

*Work performed under the auspices of the U.S. Department of Energy by the Lawrence Livermore Laboratory under contract number W-7405-ENG-48.

INTRODUCTION

A computational technique used successfully for subsurface explosion cratering (Clark and Thurston, 1976; Burton, et al., 1975; Bryan, et al., 1974; Terhune, et al., 1970; and Cherry, 1962) has been extended to meteorite impact cratering. Meteor (Barringer) Crater, located between Winslow and Flagstaff, Arizona (approximate coordinates 35°N 111°W), was selected for this computer simulation. It has also been known as the Canyon Diablo Crater, Arizona Meteorite Crater, Barringer Meteorite Crater, Coon Butte, and Crater Mound. The Canyon Diablo Meteorite, named after the nearest post office, formed the Meteor Crater. The early-time or dynamic phase of the meteorite impact was treated with a two-dimensional Eulerian finite difference code called SOIL, written by Johnson (1977). The SOIL code was a derivative of the earlier DORF and RADOIL codes (Johnson, 1970, 1971). This treatment was similar to that used in a pioneering effort by Bjork (1961), but it was extended to a time of 0.5 seconds or about a factor of ten later. Recently O'Keefe and Ahrens (1976, 1977) have reported calculations similar to that by Bjork but placed their emphasis on ejecta dynamics. In the present work, the late time or ballistic phase extrapolation was used to compute the final crater profile after the velocity field had been established in the mound region. This was done by computing an ejecta distribution based on ballistic trajectories followed by a slope stability adjustment. Parameters for the ballistic phase such as bulking factor and slope stability angle were selected from earlier explosion cratering studies (Bryan, et al., 1974).

This computational study of impact cratering was motivated by recent cratering meetings held at the U.S. Geological Survey in Flagstaff, Arizona. The Symposium on Planetary Cratering Mechanics (see Roddy, et al., 1977) was held in 1976, followed by the Impact and Explosion Cratering Workshop held in 1977. In 1961, impact and explosion cratering were topics at the Geophysical Laboratory - Lawrence Radiation Laboratory Cratering Symposium held at the Geophysical Laboratory of the Carnegie Institution in Washington, D.C., (see Nordyke, 1961).

Meteorite Impact Conditions

Table I and Figure 1 show some estimated values for the Canyon Diablo or Barringer meteorite impact velocity, mass, and kinetic energy which formed Meteor Crater, Arizona. Heide (1957) reports a range of about 15 to 45 km/s for meteorite velocities. Estimates of meteorite impact velocity were discussed by Bjork (1961) in the range between 11 and 72 km/s. Escape velocity from the earth is about 11 km/s while the largest velocity any member of the solar system can have with respect to the earth is about 72 km/s. Shoemaker (1977) reports earth-crossing asteroids with velocities with respect to earth ranging between about 15 and 40 km/s. At least some of the meteorites have asteroidal origin (Wood, 1968; Chapman, 1976; Wetherill, 1976). Based on the fact that some of the meteorite was fused by shock, Shoemaker (1963) has calculated a minimum impact velocity of 9.4 km/s. The minimum impact velocity required to completely vaporize a meteorite has been estimated to be about 14 km/s (Zel'dovich and Raizer, 1967).

Presumably a significant portion of the meteorite mass was vaporized in the formation of Meteor Crater, Arizona. Thus, the impact velocity for the Barringer meteorite was probably between about 11 and 40 km/s.

Estimates of the Barringer meteorite mass span more than two orders of magnitude (see Table I and Figure 1). Samplings of tiny spherical iron droplets in the area of Meteor Crater by Rinehart (1957) and Nininger (1956) suggest that the mass of the meteorite was at least 10^7 kg or greater (Baldwin 1963). In 1929, Moulton estimated the impact conditions as shown by the box enclosed by dashed lines in Figure 1. He calculated an impact velocity between 11 and 24 km/s and mass between 4.6×10^7 to 2.8×10^9 by considering the work required to shear rock at the crater walls, crush and pulverize the rock within the crater, and heat the meteorite and adjacent rock mass. Estimates made since 1929 have tended to be within the range of Moulton (see Figure 1).

Nininger (1961) found meteorite fragments around the area of Meteor Crater having different chemical compositions and suggested that at least five different masses were involved. He indicated that a large single mass was probably responsible for excavating most of Meteor Crater since 90 to 95 percent of the fragments appeared to have come from a single source (Nininger 1953). Despite these variations in chemical composition, results from rare gas, shock, and trace element studies have provided strong evidence that Barringer meteorite specimens found near Meteor Crater were products of a single fall (Moore et al., 1967; Kelly et al., 1974). In general, the estimates of meteorite mass have larger spread (about 1×10^7 to 2×10^9 kg) than corresponding estimates of impact velocity (about 11 to 72 km/s).

Bjork (1961) reported his calculation of Meteor Crater using an impact velocity of 30 km/s and a mass of 1.1×10^7 kg (1.1 megatons*). This calculation by Bjork is represented by the bullseye marked (I) in Figure 1. Bjork ran the calculation to a time of about 0.06 s with a target material represented by tuff. After analyzing this calculation, Bjork estimated the actual impact conditions to be on a line of constant momentum labeled, "X" in Figure 1. Lines of constant kinetic energy are also shown in Figure 1 for values of 1, 10, and 100 megatons. Shoemaker (1960) estimated values of near 1.7 megatons (I). Shoemaker and Kieffer (1974) recently raised the estimate to 4 to 5 megatons (F). Johnson (1960), Roddy, et al. (1975) and Dence, et al. (1977) have made estimates of 5.0, 4.0 and 4.8 megatons, respectively (see Table I). Values selected for the initial impact conditions in our calculation are similar to those by Shoemaker and Kieffer (1974) and Roddy et al. (1975). For our calculation, the meteorite mass, impact velocity, and corresponding kinetic energy were assumed to be 1.67×10^8 kg, 15 km/s, and 1.88×10^{16} J (4.5 megatons), respectively. This kinetic energy is comparable to an estimate for the energy expended during the great volcanic eruption (on the order of 10^{16} J) which destroyed Krakatoa in 1883 (Short, 1975). In most explosion cratering calculations, it is possible to model the energy sources to a high degree of accuracy. In contrast, the corresponding initial conditions to simulate the energy source for this impact crater calculation were very uncertain.

---

*A megaton of energy is equivalent to 4.186×10^{15} J or 10^{15} cal.

Some Calculational Assumptions

In this calculation, the meteorite was treated as a right circular cylinder with length and diameter of 30 m impacting at normal incidence to the horizontal ground surface represented by a semi-infinite half-space. These assumptions introduced a vertical axis of rotational symmetry which permitted a two-dimensional rather than a three-dimensional simulation of the impact event. Bjork (1961), who made similar assumptions, explained that based on hypervelocity experiments, impact crater shape and size do not strongly depend on projectile shape, provided that the aspect ratio (length divided by diameter) were near unity.

Materials in our calculation were described using the Tillotson (1962) equation of state description (see Table II). The nickel-iron meteorite, containing about 0.4 percent cobalt, 7.1 percent nickel, and 89.7 percent iron had a density of about 7,810 kg/m^3 (Moore et al., 1967). In the calculation, the meteorite was treated as iron of density 7,860 kg/m^3. Roddy et al. (1975) described the ejecta as about 65 percent Kaibab, 34 percent Coconino, and Toroweap, and 1 percent Moenkopi. They reported that the Kaibab formation was about 80 to 95 m thick and consisted of sandy dolomite, dolomitic limestone, and minor calcareous sandstone. Earlier Nininger (1954) reported about 55 percent Kaibab, 13 percent Coconino, and 25 percent Moenkopi based on an excavation of rubble on the crater rim. The Moenkopi, Kaibab, Toroweap, Coconino, and Supai formations at the impact site were treated simply as a single limestone material of density 2,700 kg/m^3. This density is higher than the 2,303 kg/m^3 density reported by Regan and Hinze (1975).

Limestone was selected to approximate the impact site because the description was readily available (Allen, 1967) and the Kaibab formation made up the major component of the ejecta. Shoemaker (1963) used a density of 2,650 kg/m^3 in his analysis. Earlier Bjork (1961) had used tuff, a porous volcanic rock, with a density of 1,700 kg/m^3 to model the impact site.

In this initial calculation the materials had no shear strength. Bjork (1961) argues that the hypervelocity impact was essentially hydrodynamic in nature because the pressures involved greatly exceeded the strengths of the target materials. To a certain degree this assumption was supported to a time of 0.5 seconds by our second SOIL calculation which included material strengths. In this calculation the limestone was modeled using a shear modulus of 35 GPa and a von Mises yield strength of 0.02 GPa. Preliminary analysis of results show similar behavior in these two calculations. The crater radii were essentially unchanged while the crater depth, lip height, crater volumes, and meteorite penetration depth were reduced by about 8 percent in the calculation with elastic-plastic strength. Swift (1977) has demonstrated that both crater depth and radius depend on material strength in his calculations of high-yield nuclear surface explosion cratering phenomena. He pointed out that it is important to have a greater understanding of post shock-conditioned response of rock. This understanding coupled with computational studies emphasizing times well beyond 0.5 seconds will be required to quantify the importance of material strength in the late time formation of Meteor Crater.

A small portion of the computational mesh about the impact point is shown in Figure 2 at zero time when the meteorite (iron projectile) initially strikes the ground surface (limestone target) located at Z = -200 m. The impact velocity was 15 km/s, half the 30 km/s value used by Bjork (1961). The cylindrical meteorite was 30 m in length and diameter compared with the value of 12 m used by Bjork, so that the meteorite mass was nearly sixteen times as large as the mass used by Bjork. This 30 m diameter was based on estimates by Roddy et al. (1975). At this time the meteorite was represented by 32 zones 3.75 m on each side as shown in Figure 2. This is relatively coarse zoning, at least when compared with the mass of the largest recovered meteorite fragment reported by Nininger (1961) - smallest zone mass: 1.3×10^6 kg vs largest fragment: 6.4×10^2 kg. The 100 x 100 m portion of the mesh in Figure 2 shows the rectangular zoning which was constructed using geometrically graded zone sizes increasing in both the +R and -Z directions. The outer boundaries of the calculational mesh were at about 3,000 m away from the impact point, sufficiently removed to avoid non-physical boundary effects. The SOIL grid used during the entire simulation consisted of about 11,000 zones, with 123 zones along the Z-axis and 91 zones along the R-axis. The regions above the limestone consisted of iron and void (rather than air) zones which extended to the boundary located at Z = 0 m.

Some Calculational Results

A. Dynamic Phase

Figures 3a through 3d show the calculated meteorite impact at about 0.0, 0.5, 1.0, and 1.5 ms on a 100 x 100 m portion of the grid. The velocity vectors indicate the direction of the flow with the maximum length

representing 100 m/s. Velocities exceeding the maximum value are shown as vectors with only half of an arrow head. The MKS system of units was used in most of the figures generated with the TENPLT computer graphics code (Burton and Snell, 1974). Material boundaries are shown as line segments connected at right angles. The Eulerian SOIL code permits mixed material zones or for this calculation zones which contained both iron and limestone. Tracer particles, each shown as an asterisk in Figures 3a-3h, were used to help define material boundaries and mass displacements in this Eulerian calculation. Initially, they were placed just inside the meteorite boundaries and in the limestone along planes at Z = -200, -250, -300, -350, and -400 m. Both vaporized iron and limestone began to jet upward and radially outward from the impact point. Figures 3e through 3h show the same sequence at times of about 2, 3, 4, and 5 ms. Vaporized iron with a density less than 10 kg/m^3 is labeled as a separate material. At 2 ms (Fig. 3e), the back of the meteorite is at the original ground surface. The front of the meteorite has been slowed down and compressed so that the length, originally 30 m, is now compressed to about 20 m. Between 2 and 3 ms, the average velocity of the front of the meteorite has slowed to about 8 km/s. At 3 ms (Fig. 3f), the meteorite has penetrated to a depth of about 30 m, the original length of the meteorite. In Figures 3g and 3h the meteorite is vaporizing and breaking apart. These computer-generated figures parallel the phenomenological sequence of cratering presented by Roddy (1978).

This initial calculation contained only limestone and iron materials. In the following discussion we assumed that the differences in shock impedance and other material properties across the actual material boundaries were negligible in order to infer the locations where shock metamorphism might have occurred from our calculation. Figures 4a through 4d show a similar sequence with pressure contours on a 100 x 100 m portion of the grid at times of about 0, 1, 2, and 3 ms with peak pressures of about 0, 433, 260, and 177 GPa, respectively. The peak pressure of about 433 GPa was in good agreement with Shoemaker's value (1960) of 450 GPa for an impact velocity of 15 km/s. The isobars represent pressure values of 0, 3.8, 13, and 50 GPa, respectively. The values of 3.8 and 13 GPa were selected to show regions where high pressure polymorphs of silica, coesite and stishovite, might have been formed (Kaula, 1968). Coesite and stishovite have been found at Meteor Crater and were formed by the shock wave in the Coconino sandstone originally located between the estimated depths of about 90 and 320 m below the original ground surface (Shoemaker and Kieffer 1974). Shocked Coconino Sandstone specimens from Meteor Crater have been analyzed with a transmission electron microscope by Kieffer et al. (1976) and four phases of SiO_2 have been identified: quartz, coesite, stishovite, and glass. Figures 4e through 4h show the corresponding velocity fields and pressure contours at about 5, 10, 25, and 50 ms with peak pressures of about 115, 52, 15, and 6 GPa, respectively. The shock wave began entering the Coconino sandstone located at 90 m depth at about 5 ms. The meteorite was lagging the shock front at

this time and reached this depth at about 13 ms. Figures 4e and 4f show a 200 x 200 m portion of the grid while figures 4g and 4h show a 600 x 600 m portion of the grid. Figure 5 shows peak pressure vs depth below the impact region along the Z axis. The calculated peak pressure in the Coconino sandstone is about 60 GPa at the depth of 90 m. Based on this calculation, stishovite might be formed to a maximum initial depth of about 175 m. Similarly, coesite might be formed to a maximum initial depth of about 320 m, the bottom of the Coconino Sandstone.

The energy partitioning between the iron and limestone is shown in figure 6 in terms of kinetic and internal energy for times between 1 and 100 ms. The values are expressed in percent of the total original energy. At 1 ms, the iron meteorite has about 87 percent of its original total energy (about 79 percent kinetic energy and about 8 percent internal energy). At 3.5 ms, this value has dropped to about 50 percent (about 38 percent kinetic energy and about 12 percent internal energy). At 10 ms, 83 percent of the total energy has been transferred into the limestone. At 100 ms, the limestone has about 36 percent of the original energy as kinetic energy and about 58 percent as internal energy. Some mass of the meteorite and limestone target left the calculational grid at the upper boundary at Z = 0 m located 200 m above the ground surface. This mass removed from the calculation was relatively small and included only about 2 percent of the total energy, a negligible amount compared to the total mass ejected from the crater. Essentially the entire mass of the meteorite was vaporized at late times in the calculation.

The penetration depth of the meteorite is shown in Figure 7 as a function of time. In the calculation the front of the projectile continued to penetrate downward until a depth of about 270 m was reached at about 0.3 s. At this late time the iron was a gas with a density less than about 10 kg/m^3. Kininger (1951) reported that undisturbed sediments were found by drilling to depths of about 300 to 370 m. Results for Bjorl's calculation which assumed an impact velocity of 30 km/s into the tuff are also shown. Although our calculation used only limestone in the target material, it was interesting to note the time and energy of the meteorite when it reached a penetration depth corresponding to the depth of the Coconino Sandstone (about 90 m). This occurs at a time of about 13 ms when the meteorite has transferred about 87 percent of its energy to the target material (see Figure 6). This is somewhat larger than the 30 to 50 percent values estimated by Kininger (1956).

High velocity impact experiments were performed using metal spheres and targets (Summers and Charters, 1959; Baker, et al., 1973). Summers and Charters obtained the empirical expression listed in Table III to fit their data. Using an average shock speed for the limestone of 5 km/s in this formula, we obtain a penetration depth of 290 m. This differs from our calculated value of about 270 m by about 7 percent. Using the sonic value of 3 km/s (Ackermann et al., 1970), we obtain a larger value, 439 m. Öpik (1961) estimated a penetration depth of about 320 m (see Table I for his other impact estimates).

Figure 8 shows the cavity of transient crater at 0.5 s, represented as contours of constant density with values of 10, 20, 50, 100, ..., 10,000 Kg/m^3 on a 600 x 600 m section of the grid. The contours can be used to estimate an effective depth of burst for the explosive formation of Meteor Crater. If the lower part of the cavity is fit to a hemisphere, the center lies about 85 m below the original ground surface. The meteorite boundary shown in Figure 9 at the same time also fits a hemisphere centered near the 85 m depth. Thus, even though the apparent energy source migrated downward from the surface following impact, it appears that one may use an effective depth of burst of about 85 m to compare Meteor crater with explosion craters. Estimates for the effective center of energy or apparent origin of the shock for the formation of Meteor Crater have been reported. These were about 64, 80, and 170 to 175 m by Johnson (1960), Gold (1963), and Shoemaker (1960), respectively.

The tracer particles in Figure 9 outline the cavity growth leading to the characteristic rim uplift. The overturning of this flap as it it were hinged probably would occur as a result of the material motion in the gravitational field for a calculation run to later times. Oliphant (1977) has discussed similar behavior observed in an explosion cratering calculation. This presumably led to the inverted stratigraphy observed at the crater rim as described by Shoemaker (1960) and Roddy et al. (1975).

B. Ballistic Phase

The final crater profiles were calculated using a ballistic throwout treatment followed by slope stability adjustment after the dynamic phase of the calculation which created the impact and stress wave propagation. This was accomplished using an option of the TENSOR graphics code (Burton and Snell, 1974) to post-process SOIL results at a particular time. The velocity field at 0.5 s is shown for a 2000 x 2000 m portion of the grid in Figure 10. Contour lines of constant speed (the scalar magnitude of material velocity) ranging from 10 to 1,000 m/s are shown superimposed on velocity vectors. The main shock front has passed beyond this portion of the grid and at this time is located between 2,000 and 3,000 m away from the original impact region.

The ballistic treatment assumed a constant gravitational field for earth with $G = 9.8\ m/s^2$. Each computational zone was tested to see if it had sufficient vertical velocity to reach a prescribed height, taken to be the original ground surface. If this test was satisfied the zone is considered to be part of the ejecta and its mass was added to the ejecta distribution at the appropriate range. If this test failed, the zone mass was left at that location and considered to be part of the non-ejecta. In Figure 11, the line which outlines the bottom of the cavity and terminates at the original ground surface marks the boundary between the calculated ejecta and the non-ejecta. The second profile line above it in Figure 11 shows the superimposed ejecta distribution which peaks near a radius of 500 m. The volume of the ejecta has been increased by 20 percent to account for bulking of the ejecta due to the random orientation of the ejecta masses (a bulking factor of 1.2).

Figure 12 shows the calculated final crater profile where a slope [illegible] is applied and the lower part of the crater was fit to a hyperbola. The values of 1.2 for the bulking factor and 35 degrees for the [illegible] were based on earlier explosion cratering simulations (Orphal et al., 1974). Other values of these parameters may prove to be more realistic in future impact cratering studies. The demarcation between ejecta and nonejecta is also shown in Figure 12.

Figure 13 shows the final crater calculated using a bulking factor of 1.0 (no bulking). Table IV shows that this appears to be a slightly better fit to the observed data. Effects of original bulking may have disappeared due to recompaction of the ejecta during the intervening years. Figure 14a shows final ejecta thickness as a function of range. Figure 14b shows the same plot expanded to compare with experimental values reported by Roddy et al. (1977). The calculated maximum range is about 25,000 m. A similar treatment using lunar gravity $G = 1.62\ m/s^2$ in the ballistic treatment is shown in Figure 15. The final crater profile is larger than the terrestrial crater (see Figure 12). Ejecta depth vs range is shown for the lunar case in Figure 16 which may be compared with Figure 14a.

A comparison of the calculated final crater profile from Figure 12 and the actual crater profile (Shoemaker, 1961) is shown in Figure 17. Table IV summarizes several crater dimensions from the actual event and the calculation. These calculational results are in good agreement with Meteor Crater in spite of simplifying assumptions. These results, using a meteorite mass of 1.88×10^8 kg and impact velocity of 15 km/s appear to fit the evidence although other sets of impact mass and velocity cannot be presently excluded.

Future calculational studies are planned which will use a multilayered impact site and more appropriate material descriptions for the Moenkopi, Kaibab, Toroweap, Coconino, and Supai formations. Other values of impact mass and velocity will be used in later analyses. Such detailed simulations should extend our understanding of impact crater formation when compared with the available geological evidence.

Meteor Crater and Nuclear Explosion Craters

Explosion cratering data has been used to make scaling estimates of impact kinetic energies involved in the formation of large impact craters. The following scaling approach is similar to those of Shoemaker (1960) and Roddy et al. (1975). Our approach differs slightly by considering the data base of eleven buried nuclear cratering events conducted by the United States. These events are listed in Table V (after Nordyke, 1977). Figure 18 shows scaled apparent crater radius SR_A vs scaled depth-of-burst SDOB. Apparent crater radius and yield data for each nuclear cratering event was used to calculate a kinetic energy for Meteor Crater (see the right-hand column of Table V).

The nuclear explosion sites listed in Table V are generally dry rather than wet sites which may be representative of the arid region at the Canyon Diablo impact site, although the location of the water table at the time of impact is very uncertain. Shoemaker has estimated that the impact occurred 20,000 to 30,000 years ago (see Roddy, 1977). Values shown in Table V range from about 1.7 to 46 megatons. Since Buggy was a row cratering event consisting of five charges and Sulky was deeply buried producing a mound or retarc rather than a crater, they were deleted from further considerations. Figure 18 shows significantly smaller scaled apparent crater radii for the

near surface event, Jalbaire Boy, as well as the deep event Palanquin. Because these two events predict very high energy values for W_B in Table V, they were also discarded. The average and standard deviation for W_B for the remaining seven events were 4.5 ± 1.8 megatons. This interval includes the estimates of Johnson (1960); Shoemaker and Hoffer (1974); Roddy et al. (1975); Peter et al. (1977); and Sun (1980), as listed in Table I.

Figure 19 shows scaled apparent crater depth SD_A vs scaled depth-of-burst SDOB. Roddy et al. (1975) have reported a value of 150 m for the apparent crater depth of Meteor Crater (see Table IV). Our calculated value of 194 m was deeper. The scaled experimental value fall below the curve for nuclear cratering experiments in alluvium in Figure 19. Although the scaled calculated value lies nearer the alluvium curve in Figure 19, this may be misleading because nuclear cratering data for other geologic media are not available for this scaled depth-of-burst. Roddy (1978) estimated the apparent lip crater depth, the sum of apparent crater depth and crater lip height, to be in excess of 200 m. In Figures 18 and 19, Meteor Crater falls closer to Jangle U than Teapot ESS. However, Shoemaker (1960) compared both the nuclear explosion craters Teapot ESS and Jangle U with Meteor Crater and reported that Teapot ESS possessed nearly all the major structural features of Meteor Crater. In spite of these remaining questions, the results from our preliminary comparisons are encouraging. It appears that Meteor Crater can be fit into the population of subsurface nuclear explosion craters (Figures 18 and 19) using an effective depth-of-burst of about 85 m and an energy of 4.5 megatons. Further refinements may be possible in future detailed analyses.

SUMMARY

A computational approach used to simulate subsurface explosion cratering has been extended to an impact cratering simulation of the formation of Meteor Crater, a single, bowl-shaped crater. The calculated results for a meteorite impacting at 15 km/s with a mass of 1.67×10^8 kg are in good agreement with the observed crater. Future studies are planned which will vary impact conditions and incorporate a more realistic multilayered geologic description of the impact site at Meteor Crater. Additional site characterization, such as described by Terhune and Carlson (1977) for nuclear cratering designs, may be required for detailed computer simulations. A computational fracture model developed for coal fracture and controlled blasting studies (Burton et al., 1977; Butkovich et al., 1977; and Bryan, et al., 1977) will be used in an attempt to correlate with observed fracture regions. Future studies are also planned for modeling other planetary and lunar impact craters including the larger, more complex craters with central uplift and ring features.

Computational tools, such as those demonstrated here, have proved to be very useful in design and analysis of subsurface explosion cratering. Successful explosion cratering studies have often combined well-instrumented experiments with companion theoretical analyses. In the future, it is anticipated that such computational tools will play an increasingly important role in analyses of impact cratering.

ACKNOWLEDGMENTS

We express our appreciation to Robert M. Schock and David J. Roddy who helped arouse our curiosity in the area of impact cratering and have provided continuing encouragement and support. We thank Rand B. Schaal, Dennis L. Orphal, and David J. Roddy who reviewed our manuscript and provided many helpful suggestions and criticisms. We wish to acknowledge the assistance of Lydia D. Burrow in preparing this manuscript. John A. Blunden was responsible for optical effects in the color movie used to highlight our calculation. This work was performed under the auspices of the U. S. Department of Energy under Contract No. W-7405-ENG-48.

REFERENCES

Ackermann H. D., Godson R. H., and Watkins J. S. (1975) A Seismic Refraction Technique used for Subsurface Investigations at Meteor Crater, Arizona. J. Geophys. Res. 80, 765-775.

Allen R. T. (1967) Equation of State of Rocks and Minerals. General Atomic, San Diego, CA, Report GAMD-7834. 23 pp.

Baker W. E., Westine P. S., and Dodge F. T. (1973) Similarity Methods in Engineering Dynamics: Theory and Practice of Scale Modeling. Hayden Book Co. Inc., Rochelle Park, NJ, pp 396.

Baldwin R. B. (1949) The Face of the Moon. Univ. Chicago Press. 239 pp.

Baldwin R. B. (1963) The Measure of the Moon. Univ. Chicago Press. 448 pp.

Beals C. S. and Innes M. D. (1964) Identification of Ancient Meteorite Craters. Meteoritika 25, 3-39.

Bjork R. (1961) Analysis of the Formation of Meteor Crater, Arizona: A Preliminary Report. J. Geophys. Res. 66, 3379-3387.

Bryan J. B., Burton D. E., and Denny M. D. (1974) Numerical Studies of Cratering in Bearpaw Shale: Two-Dimensional Results. Lawrence Livermore Laboratory, Livermore, CA., Report UCRL-51859. 52 pp.

Bryan J., Snell C., Heusinkveld M., Burton D., Bruce L., Lettis L., and Butkovich T. (1977) Controlled Blasting Calculations and Experiments. Energy and Mineral Resource Recovery, American Nuclear Society Topical Meeting, April 12-14, Golden, CO., U.S. Department of Energy, Report CONF-770440, 663-672.

Burton B. L., and Snell C. M. (1974) User's Guide to TEXPLT (TLESSOR Graphics Code), and PLOTLIB and MAPPLESS (Auxiliary Data Codes). U.S. Army Engineer Waterways Experiment Station, Vicksburg, MS, Misc. Paper E-74-1. 134 pp.

Burton B. E., Snell C. M., and Bryan J. B. (1975) Computer Design of High-Explosive Experiments to Simulate Subsurface Nuclear Detonations. Nucl. Tech. 26, 65-87.

Burton B. E., Lettis L. A., Bryan J. B., Butkovich T. R., and Bruce A. L. (1977) Anisotropic Creation and Closure of Tension Induced Fractures. Energy and Mineral Resource Recovery, American Nuclear Society Topical Meeting, April 12-14, Golden, CO., U.S. Department of Energy, Report CONF-770440, 673-683.

Butkovich T. R., Burton D. E., and Bryan J. B. (1977) Calculational Modeling of Explosive Fracture and Permeability Enhancement. Energy and Mineral Resource Recovery, American Nuclear Society Topical Meeting, April 12-14, Golden, CO, U.S. Department of Energy, Report CONF-770440, 654-662.

Chapman C. R. (1976) Asteroids as Meteorite Parent-Bodies: The Astronomical Perspective. Geochim. Cosmochim. Acta 40, 701-719.

Cherry J. T. (1967) Computer Calculations of Explosion-Produced Craters. Int. J. Rock Mech. Min. Sci. 4, 1-22.

Cook C. S. (1964) The Mass of the Canyon Diablo Meteorite. Nature 204, 867.

Cunningham M. E. (1974) User's Manual for the Oil Codes. Lawrence Livermore Laboratory, Livermore, CA, Report UCID-16695. 69 pp.

Dence M. R., Grieve R. A. F., and Robertson P. B. (1977) Terrestrial Impact Structures: Principal Characteristics and Energy Considerations. In Impact and Explosion Cratering (D. J. Roddy, R. O. Pepin, and R. B. Merrill, eds.), Pergamon Press, New York, 247-275.

Glenn H. D., and Thomsen J. M. (1976) Computer Simulation of a High-Explosive Cratering Experiment in a Complex Multilayered Geology. Lawrence Livermore Laboratory, Livermore, CA, Report UCRL-78155. 50 pp.

Heide F. (1957) Meteorites. Translated by E. Anders and E. Dufresne, Univ. Chicago Press. 144 pp.

Johnson G. W. (1960) Note on Estimating the Energies of Arizona and Ungava Meteorite Craters. Lawrence Livermore Laboratory, Livermore, CA., Report UCRL-6227. 18 pp.

Johnson W. E. (1970) Development and Application of Computer Programs Related to Hypervelocity Impact. Systems, Science and Software, La Jolla, CA, Report 3SR-353, ARPA Order No. 854.

Johnson W. E. (1971) RADOIL and RAM. Systems, Science and Software, La Jolla, CA, Report 3SR-104, DASA-2649.

Johnson W. E. (1977) Prepublication Communication on the SOIL Code, Computer Code Consultants, Los Alamos, NM.

Kaula W. M. (1968) An Introduction to Planetary Physics: The Terrestrial Planets. John Wiley and Sons, Inc., New York. 490 pp.

Kieffer S. W., Phakey P. P., and Christie J. M. (1976) Shock Processes in Porous Quartzite: Transmission Electron Microscope Observations and Theory. Contrib. Mineral. Petrol. 59, 41-93.

Kelly W. R., Holdsworth E., and Moore C. B. (1974) The Chemical Composition of Metallic Spheroids and Metallic Particles within Impactite from Barringer Meteorite Crater, Arizona. Geochim. Cosmochim. Acta 38, 533-543.

Kopal Z. (1966) An Introduction to the Study of the Moon. Gordon and Breach Science Publ., Inc., New York. 464 pp.

Moore C. B., Birrell F. J., and Lewis C. F. (1967) Variations in the Chemical and Mineralogical Composition of Rim and Plains Specimens of the Cañon Diablo Meteorite. Geochim. Cosmochim. Acta 31, 1885-1892.

Kiningor H. H. (1951) A Resume of Researches at the Arizona Meteorite Crater. The Scientific Monthly, LXXII, No. 2, 75-86.

Nininger H. H. (1953) A Comet Strikes the Earth. 4th Rev., Desert Press, Inc., Palm Desert, CA, 76 pp.

Nininger H. H. (1954) Impactite Slag at Barringer Crater. Am. J. Sci. 252, 277-290.

Nininger H. H.(1956) Arizona's Meteorite Crater: Past - Present - Future. American Meteorite Laboratory, Denver, CO, 232 pp.

Minings R. H. (1964) Ask a Question About Meteorites. American Meteorite Laboratory, Denver, CO, 87 pp.

Nordyke M. D., - Editor (1961) Proceedings of the Geophysical Laboratory - Lawrence Radiation Laboratory Cratering Symposium. Lawrence Livermore Laboratory, Livermore, CA, Report UCRL-6438, Parts I and II.

Nordyke M. D. (1977) Nuclear Cratering Experiments: United States and Soviet Union. In Impact and Explosion Cratering (D. J. Roddy, R. O. Pepin, and R. B. Merrill, eds.), Pergamon Press, New York.

O'Keefe J. D., and Ahrens T. J. (1976) Impact Ejecta on the Moon. Proc. Lunar Sci. Conf. 7th, p. 3007-3025.

O'Keefe J. D., and Ahrens T. J. (1977) Meteorite Impact Ejecta: Dependence of Mass and Energy Lost on Planetary Escape Velocity. Sci. 198, 1249-1251.

Öpik E. J. (1961) Notes on the Theory of Impact Craters. In Proceedings of the Geophysical Laboratory - Lawrence Radiation Laboratory Cratering Symposium (M. D. Nordyke, ed.). Lawrence Livermore Laboratory, Livermore, CA., Report UCRL-6438 Part II. S1-S28.

Orphal D. L. (1977) Calculations of Explosion Cratering - II, Cratering Mechanics and Phenomenology. In Impact and Explosion Cratering (D. J. Roddy, R. O. Pepin, and R. B. Merrill, eds.) Pergamon Press, New York. p 907-917.

Regan R. D., and Hinze W. J. (1975) Gravity and Magnetic Investigations of Meteor Crater, Arizona. J. Geophys. Res. 80(5), 776-782.

Kinsman J. S. (1[illegible]) A Soil Survey Around the Barringer Crater, Arizona. Sky and Telescope, 16, [illegible].

Roddy D. J., Pepin R. O., and Merrill R. B. - Editors (1977) Impact and Explosion Cratering - Planetary and Terrestrial Implications. Pergamon Press, New York, 1301 pp.

Roddy D. J., Boyce J. M., Colton G. W., and Dial A. L., Jr. (1975) Meteor Crater, Arizona, Rim Drilling with Thickness, Structural Uplift, Diameter, Depth, Volume and Mass Balance Calculations. Proc. Lunar Sci. Conf. 6th, p 2621-2644.

Roddy D. J. (1977) Large-scale Impact and Explosion Craters: Comparisons of Morphological and Structural Analogs. In Impact and Explosion Cratering (D. J. Roddy, R. O. Pipin, and R. B. Merrill, eds.), Pergamon Press, New York, p 185-246.

Roddy D. J. (1978) Cratering Motions for Bowl-Shaped Impact Craters: A Phenomenological Sequence of Events (abstract). Proc. Lunar Sci. Conf. 9th, p 967-969. Lunar and Planetary Institute, Houston, TX.

Shoemaker E. M. (1960) Penetration Mechanics of High Velocity Meteorites, Illustrated by Meteor Crater, Arizona. In Structure of the Earth's Crust and Deformation of Rocks, p 418-434. Intl. Geol. Cong., XXI Session, Pt. 18, Copenhagen.

Shoemaker E. M. (1961) Geological Interpretation of Lunar Craters. U.S. Department of Interior Geological Survey, Administrative Report, 139 pp.

Shoemaker E. M. (1963) Impact Mechanics at Meteor Crater, Arizona. In the Moon, Meteorites, and Comets (B. M. Middlehurst and G. P. Kuiper, eds.), p 301-336, Univ. Chicago Press.

Shoemaker E. M., and Kieffer S. W. (1974) Guidebook to the Geology of Meteor Crater, Arizona. Prepared for the 37th Annual Meeting of the Meteoritical Society. 67 pp.

Shoemaker E. M. (1977) Astronomically Observable Crater-Forming Projectiles. In Impact and Explosion Cratering (D. J. Roddy, R. O. Pepin, and R. B. Merrill, eds.), Pergamon Press, New York, 617-628.

Short N. M. (1975) Planetary Geology. Prentice-Hall, Inc., Englewood Cliffs, NJ, 361 pp.

Summers J. L. and Charters A. C. (1959) High-Speed Impact of Metal Projectiles in Targets of Various Materials. Proc. Third Sym. on Hypervelocity Impact, 101-110.

Sun J. M. S. (1970) Energy Counter-Pressure Scaling Equations of Linear Crater Dimensions. J. Geophys. Res. 75, 2003-2027.

Swift R. P. (1977) Material Strength Degradation Effects on Cratering Dynamics In Impact and Explosion Cratering (D. J. Roddy, R. O. Pepin, and R. B. Merrill, eds.), p. 1025-1042, Pergamon Press, New York.

Terhune R. W., and Carlson R. C. (1977) Site Characterization Requirements for Nuclear-Cratering Design. Lawrence Livermore Laboratory, Livermore, CA., Report UCRL-52253. 17 pp.

Terhune R. W., Stubbs T. F., and Cherry J. T. (1970) Nuclear Cratering on a Digital Computer. In Proceedings, Symposium on Engineering with Nuclear Explosives, January 14-16, Las Vegas, NV, p 334-359, American Nuclear Society and U.S. Atomic Energy Commission, Report CONF-700101 (Vol. I).

Tillotson J. H. (1962) Metallic Equations of State for Hypervelocity Impact. General Atomic, San Diego, CA, Report GA-3216, 139 pp.

Vdovykin G. P. (1973) The Canyon Diablo Meteorite. Space Sci. Rev., 14, 758-772.

Vortman L. J. (1970) Nuclear Excavation. In Education for Peaceful Uses of Nuclear Explosives (L. W. Weaver, ed.), p 65-79. The Univ. of Arizona Press, Tucson, AZ.

Wetherill G. W. (1976) Where Do the Meteorites Come From? A Re-Evaluation of the Earth-Crossing Apollo Objects as Sources of Chondritic Meteorites. Geochim. Cosmochim. Acta 40, 1297-1317.

Wood J. A. (1968) Meteorites and the Origin of Planets. McGraw-Hill Book Co., New York, 117 pp.

Zel'dovich Ya. B., and Raizer Yu. P. (1967) Physics of Shock Waves and High-Temperature Hydrodynamic Phenomena (W. D. Hayes and R. F. Probstein, eds.). Vol. 2, 845 pp. English Translation, Academic Press, New York.

TABLE I. A list of some estimates of impact mass, velocity, and kinetic energy for the Barringer Meteorite.

Source	Mass (kg)	Velocity (km/s)	Kinetic Energy (J)	Kinetic Energy (megatons)
Kinsman (1957)	$>1.1\times10^{7}$	--	--	--
Baldwin (1959)	--	--	3.0×10^{14}	0.07
Bjork (1961) calculations	1.1×10^{7}	30	4.8×10^{15}	1.1
Shoemaker (1960)	6.3×10^{7}	15	7.1×10^{15}	1.7
Beals & Innes (1964)	4.7×10^{7}	20	9.4×10^{15}	2.3
Sun (1970)	1.4×10^{8}	15	1.5×10^{16}	3.7
Roddy et al. (1975)	1.5×10^{8}	15	1.7×10^{16}	4.0
Shoemaker and Kieffer (1974)	1.7×10^{8}(a)	15(a)	1.9×10^{16}(a)	4 to 5
Dence et al. (1977)	--	--	2.0×10^{16}	4.8
Johnson (1960)	--	--	2.1×10^{16}	5.0
Kopal (1966)	2.7×10^{8}	15	3.0×10^{16}	7.2
Baldwin (1963)	2.6×10^{8}	16	3.4×10^{16}	8.1
Cook (1964)	1.9×10^{8}	30	8.4×10^{16}	20
Öpik (1961)	2.2×10^{9}	16	2.8×10^{17}	67
Öpik (1958)	2.6×10^{9}	15	2.9×10^{17}	70
THIS CALCULATION	1.7×10^{8}	15	1.9×10^{16}	4.5

(a) Estimated by authors based on 4.5 megatons and 15 km/s.

Table II. Tillotson equation of state parameters for Iron and Lithium Fluoride.

	Iron	Lithium Fluoride
ρ_o (g/cm^3)	7.86	2.70
a ( )	0.50	0.50
E_o (erg/g)	9.5×10^{10}	1.0×10^{11}
b ( )	1.50	0.60
A (erg/g)	1.32×10^{12}	4.0×10^{11}
E_s (erg/cm^3)	2.44×10^{10}	2.5×10^{10}
E'_s (erg/g)	1.03×10^{11}	1.4×10^{11}
α ( )	5.0	5.0
β ( )	5.0	5.0
B (erg/cm^3)	1.05×10^{12}	6.7×10^{11}

The Tillotson equations for the gaseous and solid regions are:

$$PGAS = \frac{aE}{V} + \left\{ \frac{b\frac{E}{V}}{\frac{E}{E_0\left(\frac{V_0}{V}\right)^2} + 1} + A\mu e^{-\alpha\left(\frac{V}{V_0} - 1\right)} \right\} e^{-\beta\left(\frac{V}{V_0} - 1\right)^2}$$

$$PSOL = \frac{E}{V}\left\{ a + \frac{b}{\frac{E}{E_0\left(\frac{V_0}{V}\right)^2} + 1} \right\} + A\mu + B\mu^2 .$$

V = specific volume = $\frac{1}{\rho}$

V_o = normal specific volume = $\frac{1}{\rho_o}$

$\mu = \frac{V_o - V}{V}$

E = specific internal energy (with radiation energy subtracted out)

PGAS = pressure of gaseous material

PSOL = pressure of solid material or of material whose specific internal energy is below the vaporization energy.

See Cunningham (1974), Allen (1967), and Tillotson (1962) for additional details.

TABLE III. Empirical penetration formula by Summers and Charters (1969).

$$P/d = 2.28 \left(\frac{\rho}{\rho_t} \frac{V}{C_t}\right)^{2/3}$$

d:	projectile diameter	30 m
ρ:	projectile density	7,860 kg/m^3
ρ_t:	target density	2,700 kg/m^3
V:	projectile impact velocity	15 km/s
C_t:	target sonic velocity	5 km/s*
P:	penetration depth	P = 290 m

*The value C_t = 5 km/s was chosen as an estimate of the average shock velocity during the first 0.5 s after impact.

TABLE IV. A comparison of calculated and actual crater dimensions for Meteor Crater, Arizona.

	ACTUAL Roddy, et. al. (1975)	CALCULATED Bulking Factor = 1.2 angle = 35°	Percent Difference	CALCULATED Bulking Factor = 1.0 angle = 35°	Percent Difference
Apparent Crater Radius (r)	518	485	-6%	505	-3%
Apparent Crater Depth (d)	150	194	+29%	194	+29%
Apparent Crater Volume (m^3)	7.60×10^7	6.35×10^7	-16%	6.99×10^7	-8%
Apparent Lip Crater Radius (r)	593	606	+2%	606	+2%
Apparent Lip Crater Height (m)	47.0*	78.0	+66%	66.9	+42%
Apparent Lip Crater Volume (m^3)	1.25×10^8	1.35×10^8	+8%	1.32×10^8	+6%

*Roddy et. al. (1975) indicate that the original crater lip height has been reduced by erosion during the intervening 20,000 to 30,000 years.

TABLE V. An energy estimate for Barringer Crater Based on U.S. nuclear cratering data.

	Medium	Yield: W (kt)	Depth of Burst DOB (m)	Apparent Crater Depth D_A (m)	Apparent Crater Radius R_A (m)	Scaled Apparent Crater Parameters SDOB $\frac{DOB}{W^{1/3.4}}$	$\frac{SD_A}{W^{1/3.4}}$	$\frac{SR_A}{W^{1/3.4}}$	Energy of Barringer Meteorite $W_B(Mt) = \frac{(R_A)_B^{3.4}}{(R_A)_1^{3.4}} \frac{W_1 (kt)}{1000}$
						m/(kt)$^{1/3.4}$			
1. Teapot ESS	Alluvium[a]	1.2	20	27	45	19	26	43	4.9
2. Danny Boy	Basalt[b]	0.42	34	19	33	44	25	43	4.9
3. Sedan	Alluvium[c]	100	194	98	184	50	25	47	3.4
4. Cabriolet	Rhyolite[b]	2.6	52	37	54	39	28	41	5.7
5. Schooner	Tuff[d]	35	108	63	130	38	22	46	3.9
6. Jangle U	Alluvium[a]	1.2	5.2	16	40	4.9	15	38	7.3
7. Neptune	Tuff[a]	0.115	31	11	31	49	21	59	1.7
8. Johnnie Boy	Alluvium[a]	0.5	0.53	9.1	18	0.6	11	22	46
9. Palanquin	Rhyolite[b]	4.3	85	24	36	55	16	23	37
10. Sulky (retarc)	Basalt[b]	0.087	27	--	--	55	--	--	--
11. Buggy (row crater)	Basalt[b]	1.1x5	41	21	38	40	20	37	7.9-40

References: Nordyke (1977); Roddy, et. al. (1975); Vortman (1970), SAMPLE: 1-7 4.5±1.8(Mt) (40%)

Water conditions:

a. Dry b. Dry (<1%) c. Dry (~20%) d. Wet (~10%) but unsaturated.

Figure Captions - Incomplete list - others on figures

Figure 3a - 3h	Velocity field; speed contours
Figure 4a - 4h	Velocity field; pressure contours

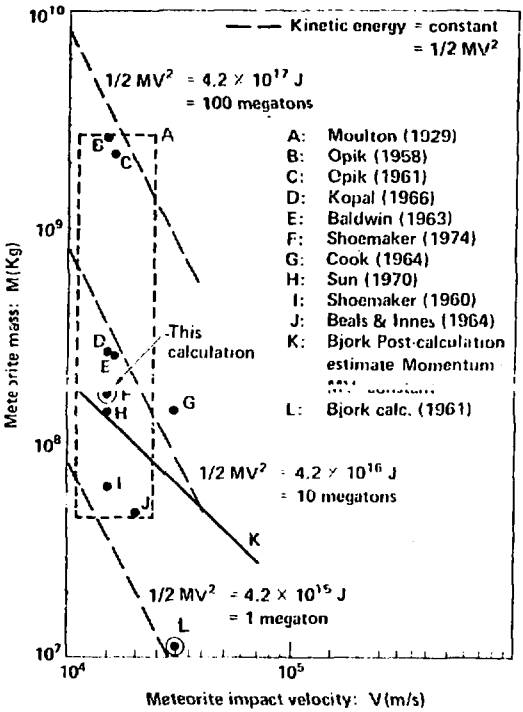

Some Estimated Impact Conditions
for Meteor Crater, Arizona

Bryan, J. B.
Crater. Sim.
Figure 1.

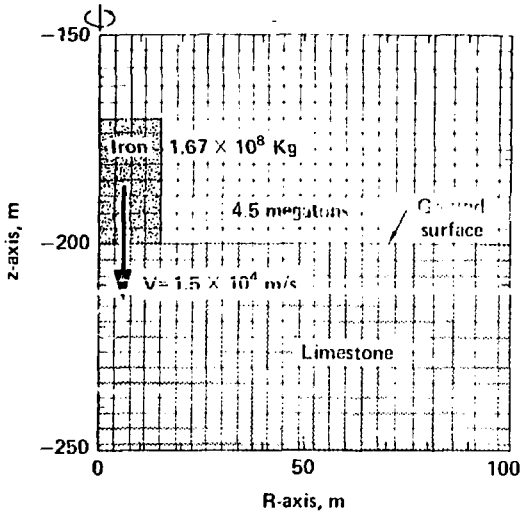

Portion of Calculational Mesh
Showing Materials Used

Bryan, J. B.
Crater. Sim.
Figure 2.

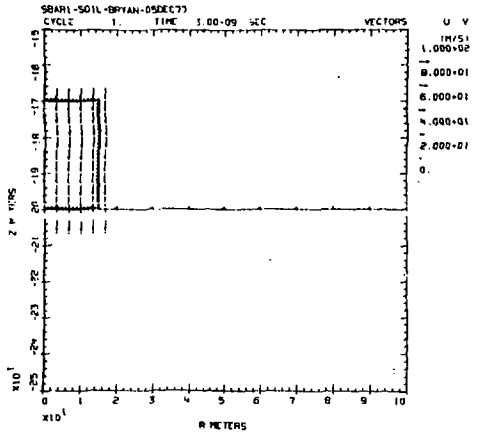

Bryan, J. B.
Crater. Sim.
Figure 3a

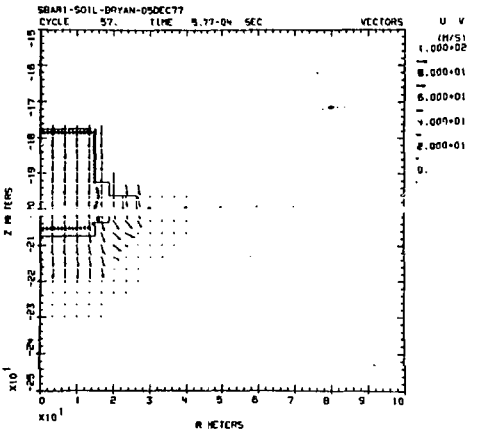

Bryan, J. B.
Crater Sim.
Figure 36

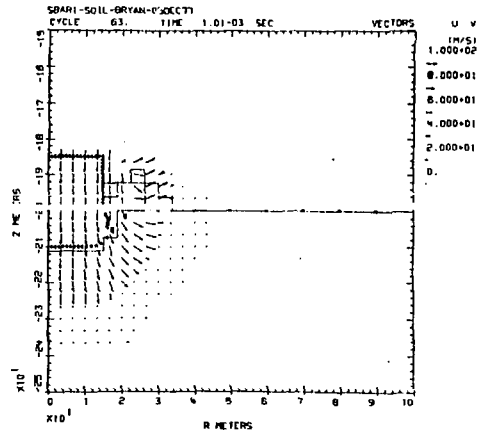

Bryan, J. B.
Crater Sim.
Figure 3c

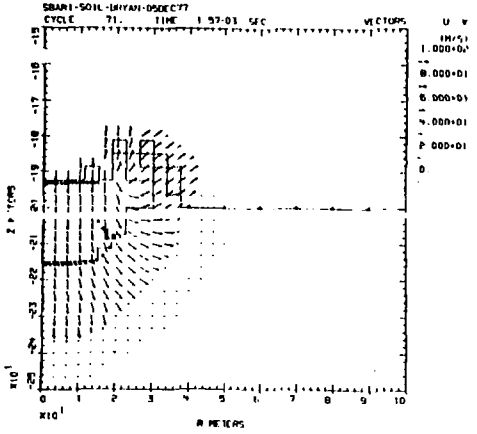

Bryan, J. B.
Crater. Sim.
Figure 3d

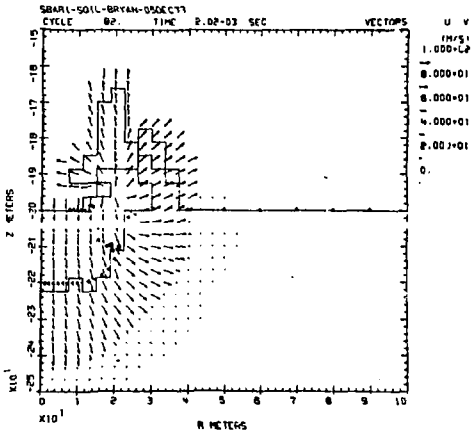

Bryan, J. B.
Crater. Sim.
Figure 3e

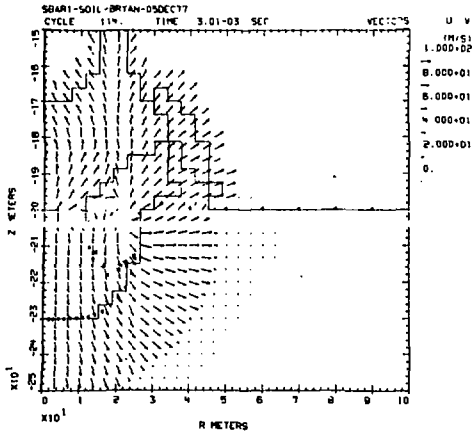

Bryan, J. B.
Crater. Sim.
Figure 3f

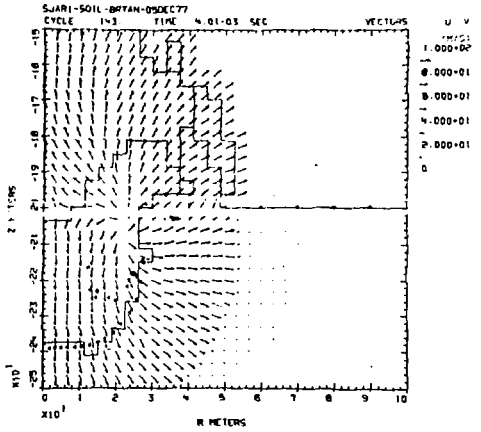

Bryan, J. B.
Crater. Sim.
Figure 3g

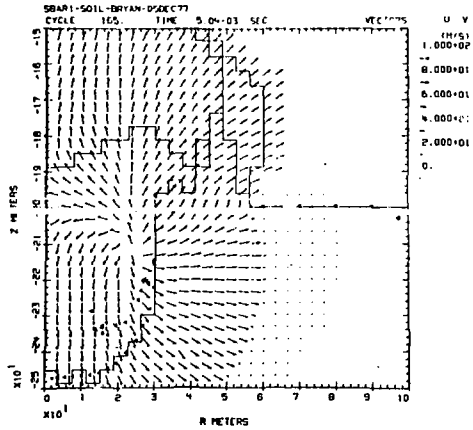

Bryan, J. B.
Crater. Sim.
Figure 3h

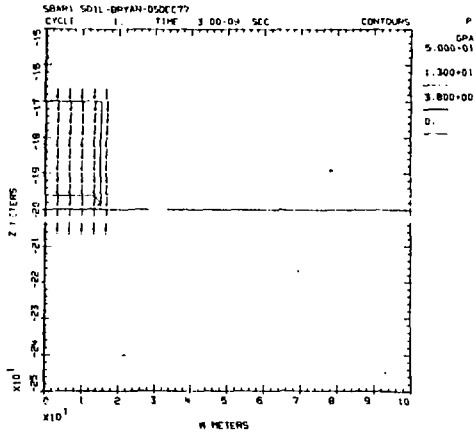

Bryan, J. B.
Crater. Sim.
Figure 4a

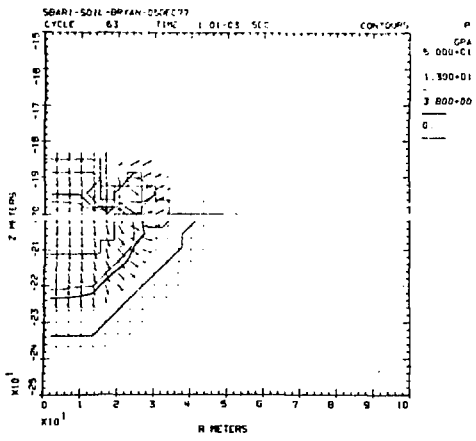

Bryan, J. B.
Crater. Sim.
Figure 4b

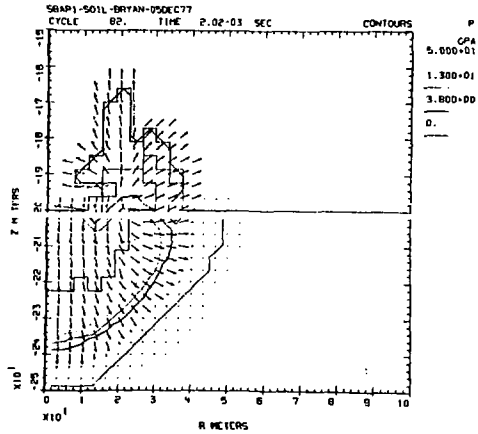

Bryan, J. B.
Crater. Sim.
Figure 4c

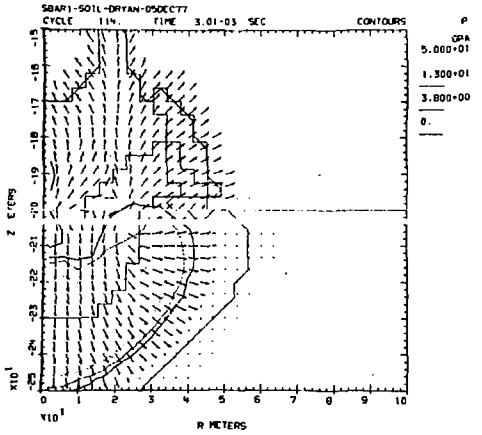

Bryan, J. B.
Crater. Sim.
Figure 4d

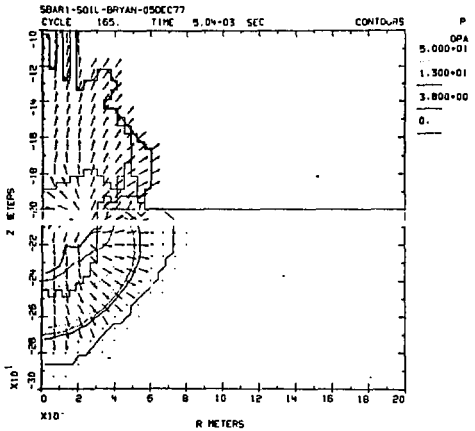

Bryan, J. B.
Crater. Sim.
Figure 4e

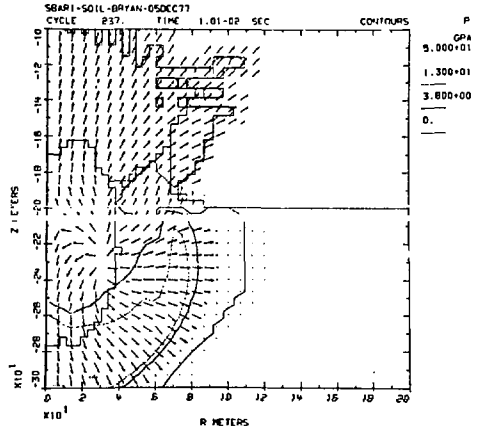

Bryan, J. B.
Crater. Sim.
Figure 4f

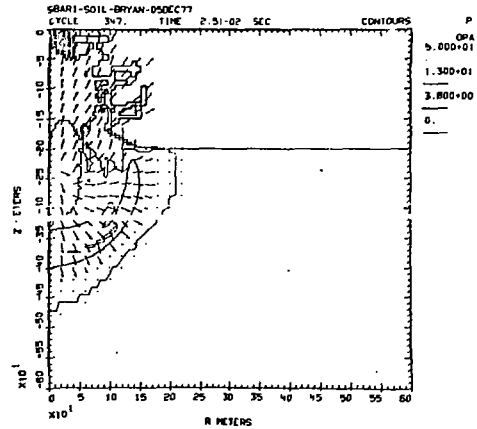

Bryan, J. B.
Crater. Sim.
Figure 4g

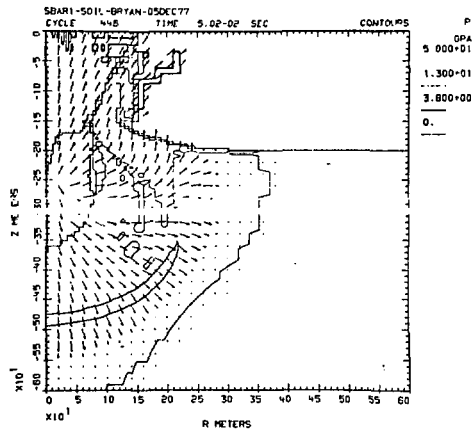

Bryan, J. B.
Crater. Sim.
Figure 4h

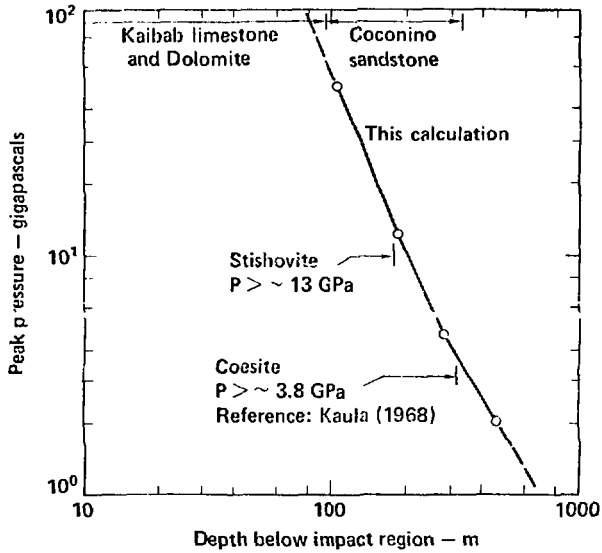

Calculated Peak Pressures Along the Z Axis

Bryan, J. B.
Crater. Sim.
Figure 5.

ENERGY PARTITIONING VERSUS TIME

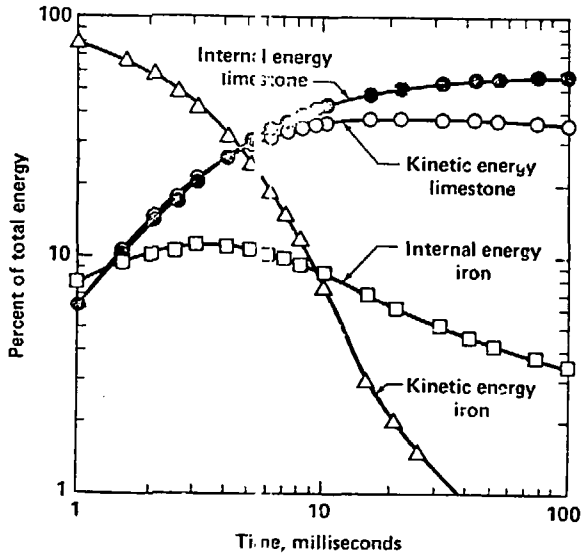

Bryan, J. B.
Crater. Sim.
Figure 6

METEORITE PENETRATION DEPTH VERSUS TIME

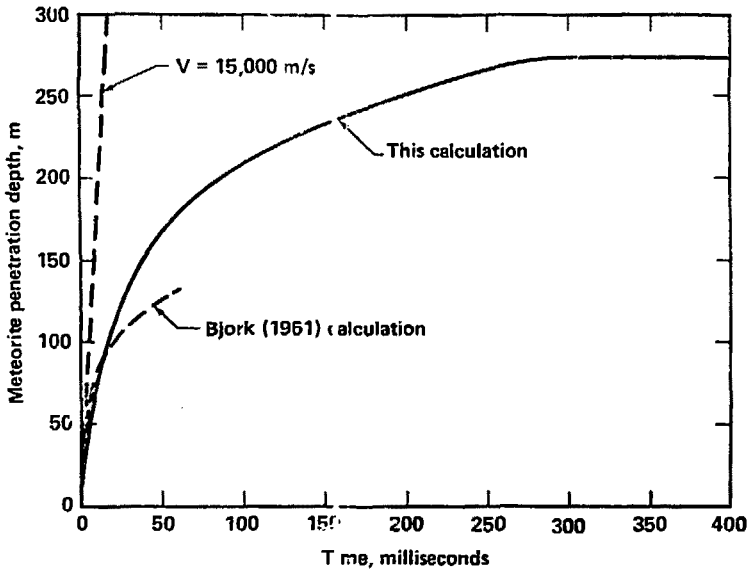

Bryan, J. B.
Crater. Sim.
Figure 7

12: CON DEN IE1 IEN L

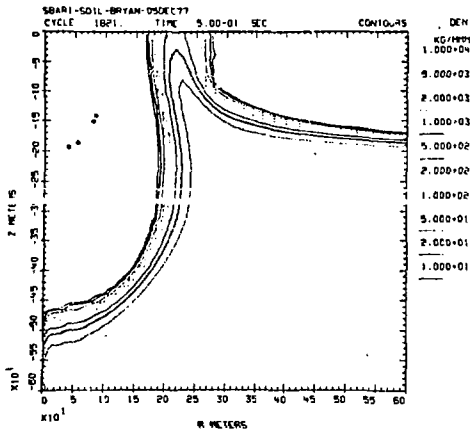

Density contours

Bryan, J. B.
Crater. Sim.
Figure 8

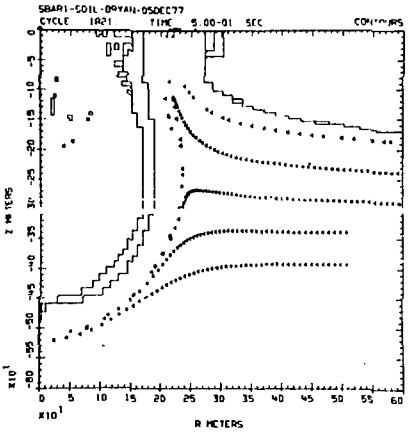

Material boundaries with
displaced tracer particles
at 0.5 seconds

Bryan, J. B.
Crater. Sim.
Figure 9

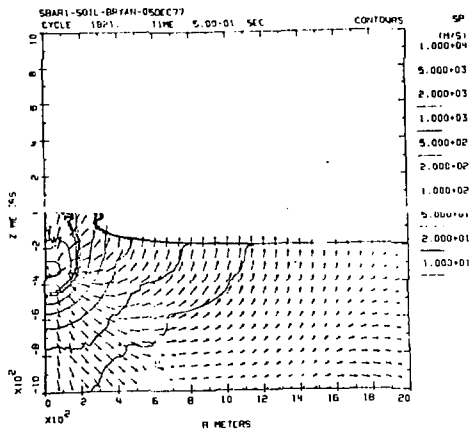

Velocity field for

ballistic throwout

Bryan, J. B.
Crater Sim.
Figure 10

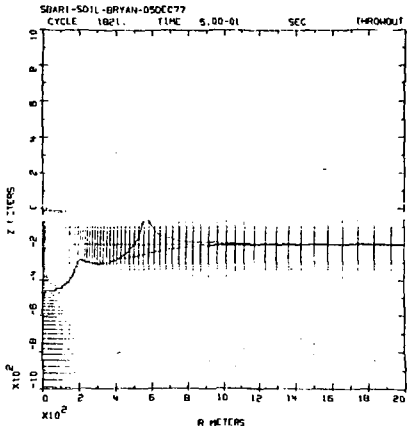

Ejecta distribution

Bryan, J. B.
Crater. Sim.
Figure 11

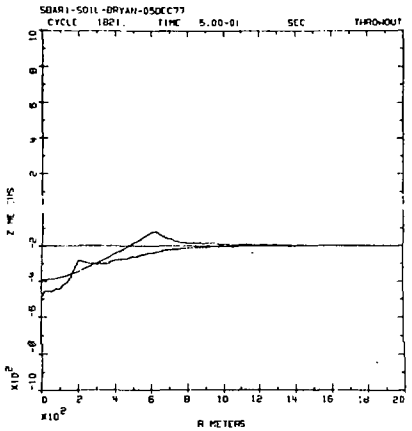

Final crater; 1.2 bulking factor

Bryan, J. B.
Crater. Sim.
Figure 12

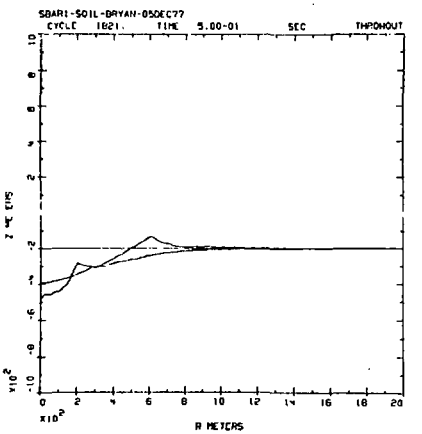

Final crater; 1.0 bulking factor

Bryan, J. B.
Crater. Sim.
Figure 13

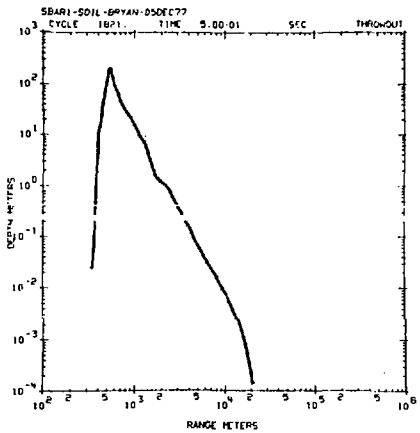

Ejecta depth versus range

Bryan, J. B.
Crater. Sim.
Figure 14a

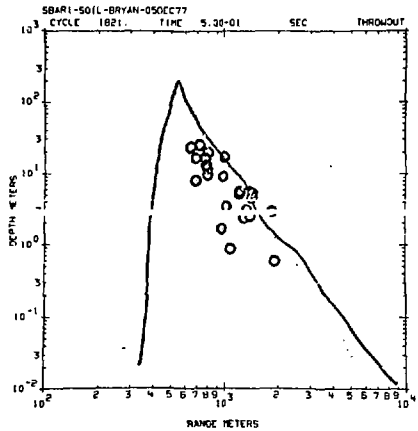

Expanded view of ejecta depth versus range

o Experimental Values from Roddy *et al.* (1975)

Bryan, J. B.
Crater. Sim.
Figure 14b

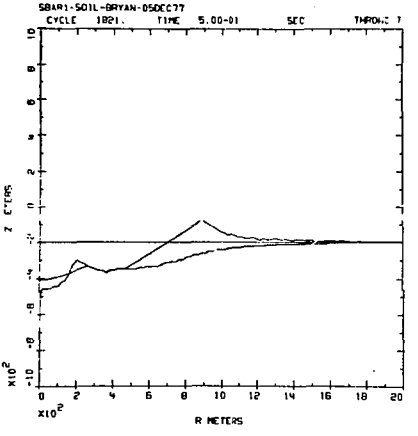

Final lunar crater;

1.2 bulking factor

Bryan, J. B.
Crater. Sim.
Figure 15

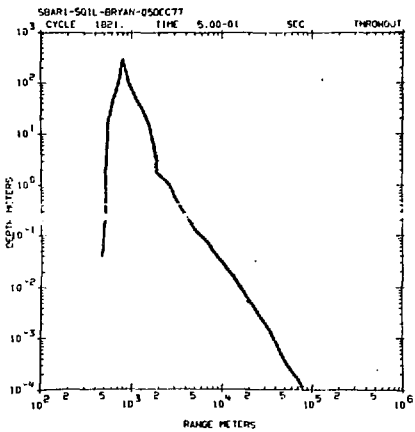

Lunar ejecta depth

versus range

Bryan, J. B.
Crater. Sim.
Figure 16

CROSS SECTION, OF METEOR CRATER, ARIZONA

(Drawn after Shoemaker, 1960)

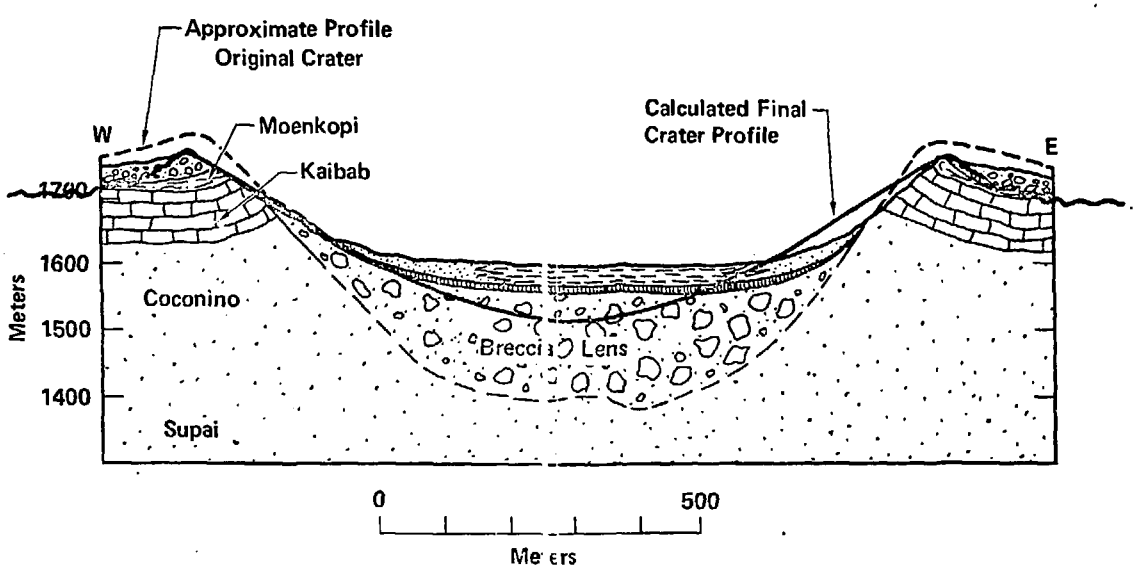

Bryan, J. B.
Crater. Sim.
Figure 17

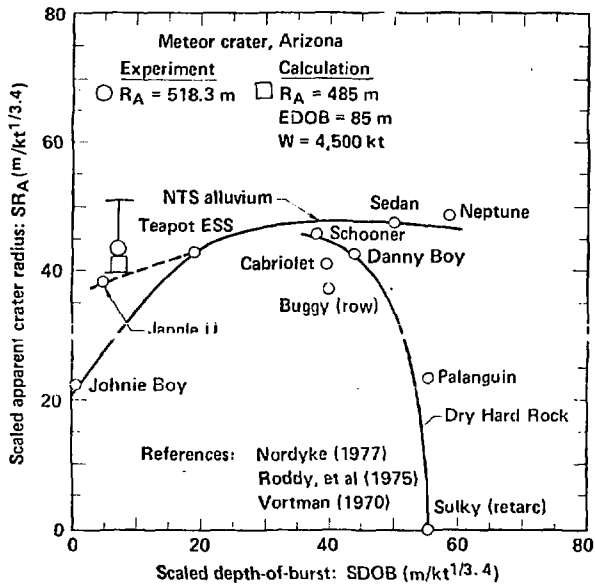

U.S. Nuclear Craters and Meteor Crater, Arizona compared using scaled apparent crater radius vs scaled depth-of-burst.

Bryan, J. B.
Crater. Sim.
Figure 18

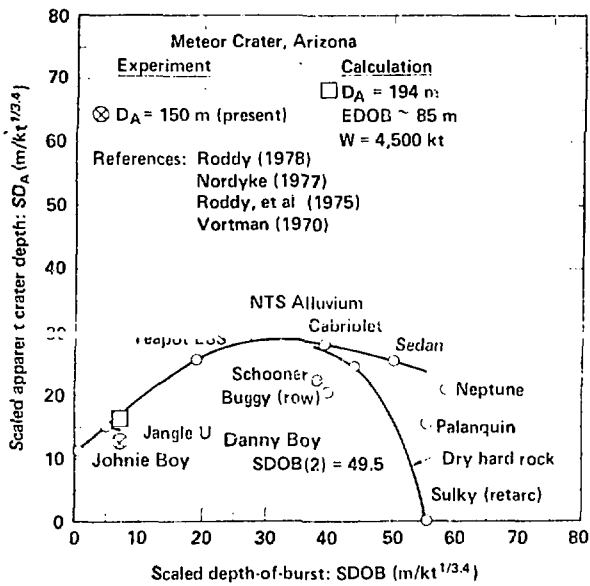

U.S. nuclear craters and Meteor Crater, Arizona compared using scaled apparent crater depth vs scaled depth-of-burst

Bryan, J. B.
Crater. Sim.
Figure 19